

The Frequency Dependent Conductivity of Electron Glasses

E. Helgren, N. P. Armistage and G. G. Bruner

Dept. of Physics and Astronomy, University of California Los Angeles, Los Angeles, CA 90095
(November 8, 2021)

Results of DC and frequency dependent conductivity in the quantum limit, i.e. $\hbar\omega > k_B T$, for a broad range of dopant concentrations in nominally uncompensated, crystalline phosphorous doped silicon and amorphous niobium-silicon alloys are reported. These materials fall under the general category of disordered insulating systems, which are referred to as electron glasses. Using microwave resonant cavities and quasi-optical millimeter wave spectroscopy we are able to study the frequency dependent response on the insulating side of the metal-insulator transition. We identify a quantum critical regime, a Fermi glass regime and a Coulomb glass regime. Our phenomenological results lead to a phase diagram description, or taxonomy, of the electrodynamic response of electron glass systems.

PACS numbers: 72.20.Ee, 71.30.+h, 71.45.Gm

I. INTRODUCTION

Disordered insulating systems have garnered much interest from theorists and experimentalists alike over many years. A plethora of results exist on the low energy physics of these disordered insulating systems from DC conductivity experiments, but it is only recently that investigations of the $T \rightarrow 0$ frequency dependent response have been performed even though theoretical predictions have existed for many years. We have measured the DC conductivity as well as the complex frequency dependent conductivity, the latter being measured in the quantum limit, i.e. $\hbar\omega > k_B T$ for a few different disordered insulating systems. Measurements were performed on materials that fall on the insulating side of the metal-insulator transition (MIT), with a major focus on the effects of electron-electron interactions. Theoretical predictions concerning the charge transport in systems with carriers localized in the Anderson sense exist both for systems without electron-electron interactions, these materials being referred to as Fermi glasses¹, as well as for systems that include the effects of the Coulomb interaction, these materials being referred to as Coulomb glasses². The majority dopant concentration of doped crystalline semiconductors and amorphous metal-semiconductor alloys can easily be varied using standard semiconductor growth techniques, and hence these materials provide a perfect playground to study the low energy electrodynamic properties of localized charge carriers.

We focus our investigation on a broad region of phase space from close to the quantum critical point, i.e. the critical dopant concentration at which the MIT occurs, x_c , to deep within the insulating regime. Recent work on the AC conductivity of Si:B³ and Si:P⁴ have shown a crossover from the Fermi glass to the Coulomb glass-like behavior qualitatively consistent with the theoretical expectations, but in all cases, the crossover is much sharper than predicted by theory. There exist two relevant energy scales in this problem. The first is the Coulomb

interaction energy, U , which Efros and Shklovskii (ES) predicted determines the crossover energy between characteristic Fermi glass and Coulomb glass-like behavior². An important result of the interactions is a depletion in the density of states of the charge carriers about the Fermi level termed a Coulomb gap. In a recent result, Lee et al.³ claim from their measurements on Si:B that the crossover energy scale is determined by the Coulomb gap width, Δ , as opposed to the theoretically predicted Coulomb interaction energy, U . Arguments based on the concentration dependence of these two parameters obtained from measurements over a broad range of dopant concentrations in another canonical electron glass system, Si:P, have recently been published by us casting doubt on this interpretation⁴. This highlights the usefulness and importance of investigating a wide range of majority dopant concentrations to fully understand these disordered insulating systems.

The primary goals of this work then are to present new data and to draw on results of previous work on other electron glass systems^{4,6} to look at the insulating side of the MIT using AC conductivity data and a broad range of dopant concentrations in order to come up with a phenomenologically supported phase diagram outlining the general classification scheme for the electrodynamic response of electron glasses. DC conductivity data are presented as well and a side by side comparison of the AC and DC data provides for unique insight. Furthermore the AC data allows for a detailed comparison of the electron glass regime with theoretical predictions. We find that some of the predicted features are observed, such as the frequency dependent conductivity power laws. In fact it is these powers that provide the taxonomic information in the phase diagram to be presented herein. We also note discrepancies that arise in all the reported measurements, such as the sharper than predicted crossovers from Fermi glass to Coulomb glass behavior.

II. BACKGROUND

A. The MIT as a Quantum Phase Transition

The metal-insulator transition is an archetypical quantum phase transition (QPT). The insulating portion of phase space associated with Fermi glass and Coulomb glass behavior borders the quantum critical regime. The quantum critical region of phase space is that region where quantum mechanical effects due to being in proximity to the zero temperature quantum critical point manifest themselves even at finite temperatures or frequencies. Specifically the electrodynamic response in a disordered electronic system, such as the lightly doped insulating semiconductors studied in this work, should smoothly transform from Fermi glass or Coulomb glass-like behavior into the appropriate quantum critical dynamic response as the dopant concentration is tuned and the MIT is approached.

For the MIT, the dopant concentration which is directly related to the charge carrier concentration, x , is typically the tuning parameter that determines whether at zero temperature the material is a metal, i.e. has a finite DC conductivity, or an insulator, i.e. the DC conductivity is zero. There exists necessarily then a critical concentration, x_c , at which the phase transition occurs thereby defining a boundary between insulating and metallic ground states. The disorder induced metal-insulator transition and the dynamical behavior near the critical point has been extensively theoretically studied over the past years both with and without electron-electron interactions^{7,10}. A thorough review has been written by Belitz and Kirkpatrick¹¹.

The condition for observing quantum critical behavior versus electron glass-like behavior on the insulating side of the MIT is determined by the relative size of certain characteristic length scales. The characteristic thermal length scale is

$$\ell_T / (k_B T)^{1/z} \quad (1)$$

and the frequency dependent length scale is

$$\ell_\omega / (\hbar \omega)^{1/z} \quad (2)$$

where z is the dynamical scaling exponent. These lengths are termed "dephasing" lengths by Sondhi et al.¹². The localization length, a measure of how far the electronic wavefunction extends, is the other important length scale. It diverges as the transition is approached and can be written in terms of concentration as

$$\ell \propto |x - x_c|^{-\nu} \quad (3)$$

where ν is the localization length exponent.

At finite temperature or frequency an intermediate regime exists between the metallic and insulating regimes that displays quantum critical (QC) behavior as shown

in Figure 1. In the QC regime the localization length is greater than the dephasing length scales, $\ell_T, \ell_\omega < \ell$. At the crossover from QC to the insulating regime this can be thought of heuristically as the electron scattering within a length scale that is shorter than the width of the wavefunction envelope that describes how localized that electron is. In other words the electron can undergo scattering akin to normal transport before "realizing" that it is localized. On the metallic side, the relevant length scale is commonly taken to be the screening length. In the opposite limit, $\ell_T, \ell_\omega > \ell$, the system exhibits metallic or insulating behavior. For instance in the insulating regime, the material will display the appropriate hopping conduction consistent with the DC conductivity or the photon assisted frequency dependent conductivity. A schematic representation of the phase diagram showing the regime boundaries is shown in Figure 1.

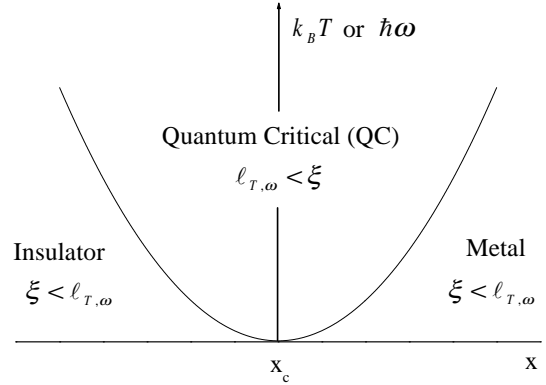


FIG. 1. A schematic of the crossover diagram close to a quantum critical point showing the regime boundaries between quantum critical, metallic and insulating behavior. The horizontal axis represents increasing concentration and the vertical axis represents either the temperature or frequency energy scale. The crossover from QC to either metallic or insulating behavior is determined by when the length scales are equivalent, i.e. $\ell_T, \ell_\omega = \ell$.

From equations (1), (2) and (3) we can determine a functional form, in terms of concentration, for the crossover between the QC and the metallic or insulating regimes by setting the dephasing length equal to the relevant length scale, $\ell_T, \ell_\omega = \ell$. In so doing we find

$$\hbar \omega_{QC} / k_B x_c^{\nu} : \quad (4)$$

In this work the approach to criticality from the insulating side of the MIT for two types of disordered insulators, SiP and NbSi, will be compared and discussed.

Mott first noted that at low temperatures in a lightly doped disordered semiconductor a form of DC conduction unique from nearest-neighbor hopping would occur¹³. It is commonly referred to as variable range hopping (VRH). Mott's derivation did not include electron-electron interactions and thus Mott-type hopping describes the variable range hopping mechanism in a non-interacting Fermi glass¹. In Mott's theory:

$$\sigma_{dc} \propto \exp[-(T_0/T)^{1/(d+1)}] \quad (5)$$

where d is the effective spatial dimension for the hopping electrons. The characteristic Mott temperature is given by

$$T_0 = \frac{1}{k_B} N_0^{-d} \quad (6)$$

It is the characteristic energy scale of the level spacing in a volume V , and dependent on the density of states (DOS), N_0 . Here $\frac{1}{k_B}$ is a constant of order one.

The above derivation was based on the assumption of an approximately constant density of states near the Fermi level, but as pointed out by Pollak¹⁴ and Ambegaokar¹⁵, this assumption is invalid when correlation effects are included. Upon including electron-electron interactions one finds that the Coulombic repulsion is responsible for opening up a gap at the Fermi energy, and that the functional form for the DC conductivity takes on an alternate temperature dependence. This gap, termed the Coulomb gap by Efros and Shklovskii¹⁶ is given by

$$E_g = \frac{e^3 N_0^{1/2}}{\epsilon_1^{3/2}}; \quad (7)$$

where ϵ_1 is the full dielectric constant. The Coulomb gap is a "soft" gap in the density of states near the Fermi level created by the Coulomb interaction between localized electrons. (The term soft is used because the density of states vanishes only at the Fermi energy.)

Efros and Shklovskii followed Mott's derivation for the DC temperature dependent VRH conductivity, but instead of using a constant density of states around the Fermi level, they incorporated the Coulomb gap and therefore necessarily took correlation effects into account. The appellation Coulomb glass describes an electron glass system which incorporates Coulombic interactions. In so doing ES found the following form for the DC temperature dependent VRH conductivity

$$\sigma_{dc} \propto \exp[-(T_0^0/T)^{1/2}] \quad (8)$$

where the characteristic ES temperature is given by

$$T_0^0 = 2.8 e^2 / k_B \epsilon_1 \quad (9)$$

The prefactor 2.8 is calculated from percolation threshold models^{17,18}. Note that the power in Eq. (8) is $\frac{1}{2}$ in all dimensions unlike in Mott's formalism.

For the system we are studying, any given sample with a particular dopant concentration may possibly exhibit more than one type of behavior. Depending on the energies at which one is probing the system one might observe behavior consistent with Fermi glass, Coulomb glass or QC-like behavior. Therefore, by investigating a broad range of frequency or temperature space, our experimental window might be broad enough to see crossovers from one type of behavior to another.

The most indicative piece of experimental evidence that most authors cite as to whether the materials being studied are Fermi glasses exhibiting Mott VRH or Coulomb glasses exhibiting ES VRH is the DC conductivity. The vicissitudes of using this experimental data to claim a material is a Coulomb or Fermi glass lie in the fact that only below a certain temperature does a material enter the VRH regime, whereas above this cut-off temperature other forms of activated hopping occur. Thus only a small portion of low temperature data will show any semblance of VRH behavior, and in three dimensions, a small section of temperature dependent data may fit a power law of $\frac{1}{2}$ or $\frac{1}{4}$ almost equally as well making it difficult to say with any certainty which mechanism of charge excitation is occurring. Measurements of the $T \rightarrow 0$ K frequency dependent conductivity then allows for new insight into the MIT and the electrodynamics of electron glasses. Measurements of the DC conductivity on the same samples as those on which the AC conductivity measurements were taken offers a consistency check with previous investigations and allows for comparison of salient features.

C . A C Photon-assisted Hopping

Mott proposed a form for the $T = 0$ K photon-assisted frequency dependent hopping conductivity for the case of non-interacting electrons based on the theory of resonant absorption using a simple one electron model of a disordered system, commonly referred to as the pair approximation^{1,19}. The resulting real part of the AC conductivity, σ_1 , in Mott's formalism is as follows:

$$\sigma_1 = e^2 N_0^{2/5} h^{1/2} [\ln(2I_0/h)]^4; \quad (10)$$

Here $\frac{1}{2}$ is some constant close to one, and I_0 is the prefactor of the overlap integral (commonly taken to be the Bohr energy of the dopant²⁰). Most notably we see that in Mott's formalism, the conductivity has an approximately quadratic frequency dependence, plus logarithmic corrections.

By taking into account the mean Coulomb interaction between two sites forming a resonant pair

$$U(r_i) = e^2 / \epsilon_1 r_i \quad (11)$$

where $r_1 = [\ln(2I_0/h!)]$ is the most probable hop distance between pairs, Efros and Shklovskii derived the real part of the AC conductivity to be:

$$\sigma_1 = e^2 N_0^{2/5} [\ln(2I_0/h!)]^4 [h! + U(r_1)] \quad (12)$$

This formula takes on a different frequency dependence in two limiting cases. In the case where the photon energy is greater than the Coulomb interaction energy, $h! > U(r_1)$, one retrieves the same approximately quadratic frequency dependence in Mott's formula (10), and here the Coulomb glass is indistinguishable from the Fermi glass in so far as the frequency dependent conductivity is concerned. For the alternate case i.e. when the photon energy is smaller than the Coulomb interaction energy, $h! < U(r_1)$, the conductivity of a Coulomb glass will show an approximately linear dependence on frequency, plus logarithmic corrections. Model data for this functional form is shown in Figure 2 showing that the crossover is predicted to occur over many decades of frequency.

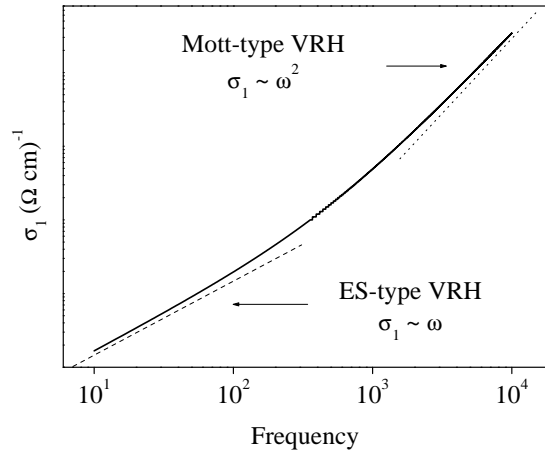


FIG. 2. A schematic of the crossover function from Mott to ES-type AC conduction set forth by Efros and Shklovskii and defined in Eq. (12) displayed on logarithmic axes. The vertical axis is conductivity with arbitrary units and the horizontal axis has been set to show the crossover occurring in the millimeter-wave range if the units are taken to be GHz. The dashed and dotted straight lines show the asymptotically approached linear and quadratic dependencies of the crossover function.

As for the DC case, one further ramification of including electron-electron interactions is the depletion of the single particle density of states around the Fermi level, i.e. the Coulomb Gap. In the special case when $U(r_1) > h!$ Efros and Shklovskii calculated the real part of the frequency dependent conductivity and obtained

$$\sigma_1 = \frac{1}{10} \frac{h!^2}{\ln(2I_0/h!)} \quad (13)$$

so that the dependence is slightly super-linear, assuming a frequency-independent dielectric constant, and inde-

pendent of the localization length, which would indicate a very weak concentration dependence.

Thus, by using the frequency dependent conductivity one has a unique means to determine the relevant energy scales between interacting and non-interacting behavior. Several recent experiments^{3,21} have shown a possible crossover from interacting to non-interacting behavior in the same material. Some of this experimental data has been interpreted to indicate that the Coulomb gap width energy scale, certainly another germane energy scale in the system, sets the crossover energy scale in opposition to the theoretical prediction that the Coulomb interaction energy dictates the crossover from Fermi glass to Coulomb glass-like behavior. These arguments though were based on measurements covering a limited range of dopant concentrations. Therefore the frequency dependent conductivity measured in the low energy excitation range for a broad range of concentrations can provide useful information about the crossover energy scale, be it the Coulomb gap width or the Coulomb interaction energy.

III. EXPERIMENTS

Experiments were performed on nominally uncompensated phosphorous doped silicon samples that were cut from a boule grown by Recticon Enterprises Inc. to a specification of 5 cm in diameter with a majority dopant gradient along the axis. This boule, grown using the Czochralski method, was subsequently sliced into 1 mm thick wafers. By the nature of the Czochralski method for growing a crystal, there is an inherent gradient in the majority dopant concentration along the axis of the boule. A greater range of variation in this dopant concentration along the axis of the boule can be achieved by continuously adding progressively more dopant of choice, in our case phosphorous, to the molten silicon as the ingot is being drawn from the liquid mixture. As summarized in the first column in Table I, we obtained samples spanning a majority dopant concentration from $1.37 \times 10^{18} \text{ cm}^{-3}$ to $2.98 \times 10^{18} \text{ cm}^{-3}$. The middle column lists the ratios of the samples as a percentage of the dopant concentration in each sample relative to the critical concentration at which the MIT occurs, $x_c = 3.5 \times 10^{18} \text{ cm}^{-3}$. The final column lists the room temperature resistivity of each sample in $(\Omega \text{ cm})$ measured using an ADE 6035 resistivity gauge, which can be directly related to the dopant concentration, knowing the bulk of majority dopant in the silicon via a phenomenological scale set forth by Thurber et al.²².

Previously reported results from another electron glass system, namely amorphous NbSi, will be drawn upon when discussing the general features of the electron glass phase diagram. These samples were created by sputtering onto sapphire substrates, and both millimeter-wave and DC conductivity measurements were performed,

$x \cdot 10^{18} \text{ cm}^{-3}$	Percent of C critical: $\frac{x}{x_c}$	$\rho_{dc} (300 \text{ K}) (\text{ cm})$
2.98	85%	0.0133
2.66	76%	0.0142
2.42	69%	0.0150
2.17	62%	0.0159
1.96	56%	0.0168
1.74	50%	0.0179
1.56	45%	0.0189
1.37	39%	0.0202

TABLE I. The material parameters for eight SiP samples obtained from a boule grown by Recticon Enterprises Inc. The left hand column lists the concentration of the majority dopant phosphorous in each sample. The middle column lists the ratio as a percentage of the dopant concentration in each sample relative to the critical concentration of the MIT, namely $x_c = 3.5 \cdot 10^{18} \text{ cm}^{-3}$. The right hand column lists the value of the room temperature DC resistivity value for each sample.

analogous to those done on SiP. More detailed sample specifications for these amorphous metal-semiconductor alloys and experimental results can be found in the literature⁵.

It is important to perform DC conductivity measurements on the same SiP samples for which the AC measurements were done for a number of reasons. First, the DC measurements offer a consistency check to previous experimental results. Also, one can compare important parameters, such as the localization length, as determined separately from the DC and AC data. These measurements also provided a low temperature value of the DC conductivity to which one can normalize the real part of the microwave resonant cavity complex conductivity. For example, at approximately 25 K the real part of the conductivity measured at the center frequencies of the resonant cavities, namely 35 GHz and 60 GHz, should be dominated by the thermally driven charge transport mechanism that determines the DC conductivity.

DC conductivity measurements were performed on the SiP samples using a standard four probe measurement technique from liquid ⁴He temperature up to approximately 100 K. Figure 3 shows data from three samples from 4.2 K up to 20 K. At the higher temperatures shown in the main portion of the figure for the 69% sample, and also evident in the inset plot of the 56% sample measured up to approximately 200 K, the curves show a rounding off indicative of a conduction process consistent with a Boltzmann type activation. Also evident in the middle of the displayed temperature range is a kink in each of the sample's data indicative of a crossover from one form of activation to another. Usually the crossover temperature, T_x , for each of the samples decreases with increasing dopant concentration. This would be consistent with a crossover from Mott to ES-type VRH, but other experimental evidence, to be discussed presently,

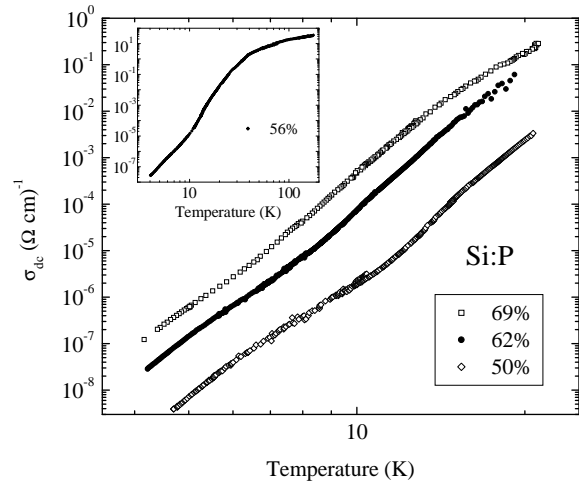


FIG. 3. The DC conductivity versus temperature on logarithmic scales for a series of SiP samples. At high temperatures one can notice a crossover to activated Boltzmann-type behavior. Also noticeable is a crossover temperature, T_x , in the middle of the displayed temperature range that decreases with increasing dopant concentration.

indicates that Mott and ES-type VRH theories do not correctly describe the upper and lower pieces of the DC conductivity data shown in Figure 3.

Figure 4 shows the measured DC conductivity from the 62% sample both prior to and after etching in a 4% HF + 96% HNO₃ solution for 20 minutes. Unless otherwise specified all AC and DC conductivity measurements reported herein were performed on etched SiP samples. As first pointed out by Otuka et al.²³, a crystalline semiconductor sample sliced from a boule using a diamond saw will create surface defects. As indicated in the figure, at low temperatures the surface defects seem to provide a channel for conduction with less resistance than the surface defect-free bulk sample, increasing the overall measured bulk conductivity. DC conductivity measurements on samples etched for 20 minutes and 2 hours showed no difference indicating that 20 minutes of etching succeeded to remedy the effects of surface defects, consistent with the findings of Otuka et al.²³. Regardless of the presence of surface defects altering the relative magnitude of the measured bulk conductivity, the kink in the data indicating a crossover temperature, T_x , is still clearly present in both sets of data.

Both components of the complex frequency dependent conductivity were determined from transmission measurements using a technique called quasi-optical spectroscopy. Quasi-optical spectroscopy has been utilized and partially developed by our research group to investigate the electrodynamic response of materials in the millimeter to sub-millimeter wave range (i.e. the terahertz frequency regime)^{24,25}. Historically the millimeter and sub-millimeter wave spectral range, higher in fre-

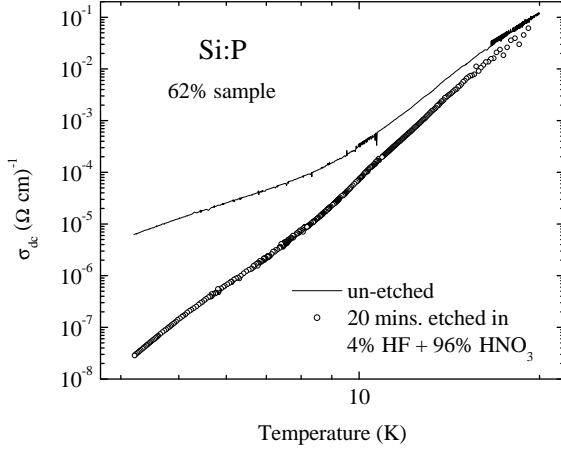


FIG. 4. The DC conductivity versus temperature on a logarithmic scale for the 62% Si:P sample both prior to and after etching the sample.

quency than standard radio-frequency (RF) techniques and lower in frequency than common infrared (IR) techniques, has not been studied, leaving a gap in the knowledge of the optical response of physically intriguing systems. This spectral range corresponds with the range of energies wherein electron-electron interactions are predicted to occur in disordered systems. Also experiments in this spectral range can easily be done in the quantum limit, $\hbar\omega > k_B T$, with standard cryogenic techniques, i.e. a pumped liquid ^4He optical cryostat (recall that $1\text{ K} \approx 20\text{ GHz}$).

The quasi-optical transmission measurement technique takes advantage of broadband sources of coherent electromagnetic radiation known as Backward Wave Oscillators (BWO). The frequency of the output radiation from these sources can be swept by adjusting the applied potential. The resulting output power spectrum is extremely reproducible. Recording the power received at the detector for 1) the sample and then 2) a blank or free space, and taking their ratio provides the transmission data as a function of frequency. The striking feature of the transmission spectra is the periodically spaced peaks known as Fabry-Perot resonances which occur whenever the thickness of the sample is equal to an integer number of half wavelengths inside of the sample. The transmission can be recorded and the resonant peak's center frequencies and heights can be determined. From these measured parameters one can directly determine the real and imaginary components of the complex conductivity.

Below a certain temperature, it was found that the Fabry-Perot resonance transmission traces did not change. This necessarily means that below some temperature the real and imaginary components of the complex conductivity, become temperature independent. At low temperatures thermal contractions, which can affect both

the peak heights and center frequencies become negligible as well. Figure 5 shows this trend by plotting the conductivity of the 69% sample versus temperature for various constant frequencies with the DC conductivity. It is clear that at high temperatures the AC conductivity curves approach and follow the temperature dependent DC conductivity, and the greater the frequency of a particular curve, the greater the temperature at which this occurs. It is also clear that the iso-frequency curves do indeed attenuate at low temperatures, indicating that the $T = 0\text{ K}$ photon-assisted hopping behavior is being observed. All of the other samples showed a similar attenuating out of the AC conductivity at low temperatures.

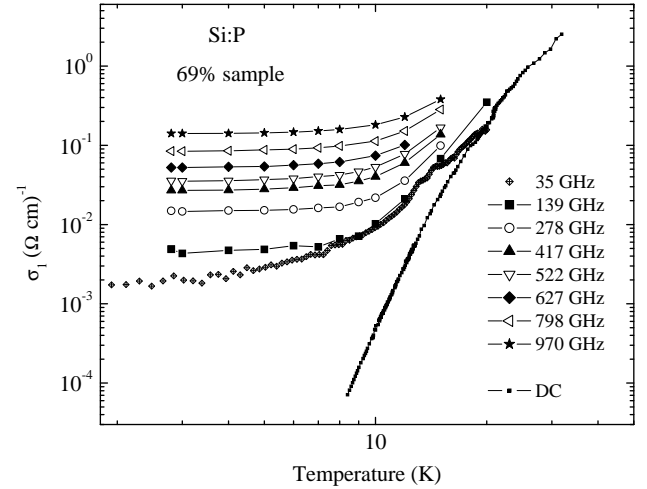


FIG. 5. Both the DC conductivity and the real component of the complex conductivity at various constant frequencies versus temperature on logarithmic scales for the 69% sample.

Using DC data alone, evidence of the effects of electron-electron interactions, namely a crossover from Mott to ES type VRH is questionable at best. The range of temperature across which the various conduction processes might be occurring are minimal and it is difficult to have confidence that a Mott-type $T^{1=4}$ behavior or ES-type $T^{1=2}$ behavior is correct. The distinguishing features of an interacting versus a non-interacting disordered system are much easier to tell apart when investigating the frequency dependent conductivity though. Specifically, linear and quadratic power law are clearly discernable and evidence for such a crossover in the frequency dependent conductivity spectrum is clearly seen as shown in Figures 6 and 7.

IV. ANALYSIS AND RESULTS

A. DC Conductivity

Much of the story that the DC conductivity can tell is summarized in Figure 8 which shows the DC conductivity of the 50% Si:P sample. The data in the upper

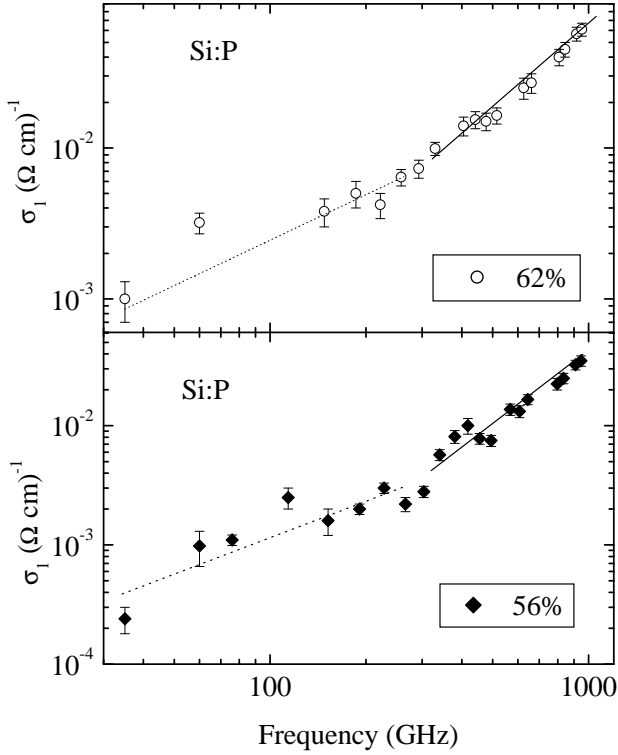


FIG. 6. The measured 2.8 K value of the real part of the complex frequency dependent conductivity for the Si:P 62% and 56% samples plotted versus frequency on logarithmic axes displaying a crossover in the type of conduction mechanism. The dashed line is a fit to the lower portion of the data and follows a nearly linear power law. The solid line through the upper portion of the data is a fit of that data and follows a nearly quadratic power law.

panel is plotted on a $T^{-1/4}$ axis in order to assist visual recognition of Mott type VRH behavior. The lower panel shows the sample data plotted on a $T^{-1/2}$ axis in an attempt to elucidate any region of data that might be following ES type VRH behavior. When plotted on any inverse temperature scale, the left hand side represents the high temperature region, and it is this higher temperature region, up to approximately 25 K, that has been fitted to a linear function in the upper panel. However, closer inspection of Figure 8 reveals that in the upper panel, although the higher temperature data has been fitted to $T^{-1/4}$ behavior, the lower portion seems to be linear as well indicating a possible $T^{-1/4}$ dependence as well on this semi-log plot. In the lower panel of Figure 8, the lower temperature data is fitted to a linear function, possibly indicating that in this region, i.e. below $T_x \approx 12$ K, the data might well be described as following ES type behavior. As in the upper panel, the other region of data, in this case the higher temperature

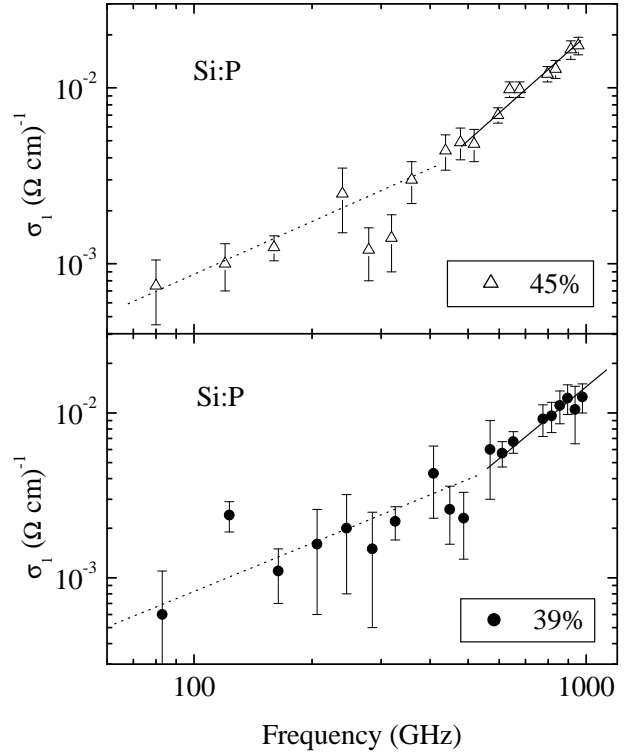


FIG. 7. The measured 2.8 K value of the real part of the complex frequency dependent conductivity for the Si:P 45% and 39% samples plotted versus frequency on logarithmic axes displaying a crossover in the type of conduction mechanism. The dashed line is a fit to the lower portion of the data and follows a nearly linear power law. The solid line through the upper portion of the data is a fit of that data and follows a nearly quadratic power law.

data, shows a somewhat linear dependence at least over a finite range of temperature.

That the upper and lower portions of the data seem linear on either scale summarizes the vicissitudes of trying to determine Mott or ES type behavior from the DC data alone. From Figure 8 one sees that the Si:P 50% sample has a crossover temperature of approximately 12 K, whereupon the DC conductivity begins to follow a different dependence. It is unclear if this temperature sets the energy scale at which a crossover from Mott to ES type VRH occurs, but nevertheless it is clearly an important energy scale in this model disordered system.

Further analysis shows that fitting the high temperature and low temperature portions of σ_{dc} respectively to Mott and ES-type functional forms, across our experimentally accessible temperature range, is incorrect. The characteristic Mott temperatures, T_0 , determined for our Si:P samples is of the order 10^7 K, a ridiculously large value. The ES characteristic temperatures, T_0^0 , deter-

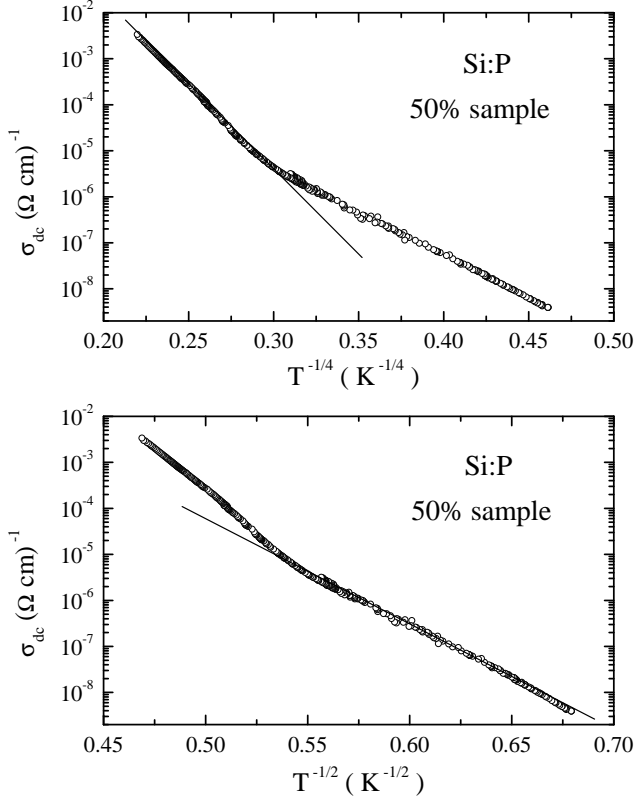


FIG. 8. The DC conductivity for the 50% Si:P sample plotted versus $T^{-1/4}$ in the upper panel and plotted versus $T^{-1/2}$ in the lower panel.

mined by fitting the lower temperature data are more reasonable but still extremely large, of the order 10^3 K. Compared to the characteristic Mott and ES temperatures measured by Dai et al.²⁶ and Homung et al.²⁷, our values seem extremely high and unphysical, even though their materials were of a different composition, or fell in a different range of dopant concentrations.

Further evidence that the Mott and ES functional forms are inappropriate can be gleaned from analysis of the localization lengths from the characteristic temperatures. Using the relationship for the ES characteristic temperature, i.e. Eq. 9 and the measured values of T_0^0 , the localization lengths for the various Si:P samples within our doping range come out to be less than 2 nm, not an unreasonable length scale as the interatomic spacing in the diamond structure lattice of Si is 2.35 Å, but an order of magnitude smaller than the 20 nm found from analyzing the AC conductivity data, to be presented in the following section. With an appropriate estimate of the noninteracting density of states $N_0(E_F)$, an estimate of the localization length can also be determined from T_0 . For example the 62% sample, with a $T_0 = 39 \times 10^6$ K, estimating $N_0(E_F)$ to be the ratio of the dopant atomic density $x = 2.173 \times 10^{24} \text{ m}^{-3}$

to an appropriate bandwidth, 0.1 eV, gives a localization length of approximately 6 Å, a factor of 4 smaller than the one determined from T_0^0 . That the localization lengths do not agree gives further evidence that 1) either our assumptions of what regions of the DC conductivity correspond to Mott or ES type VRH are incorrect or that 2) deep in the insulating regime behavior different than that predicted for canonical Coulomb and Fermi glasses exists.

The former case may well be true, (although evidence from the AC conductivity measurements seem to indicate otherwise), and these issues will be discussed presently, but first the latter issue shall be addressed. In fact such a prediction that deep in the insulating regime an alternate method of charge transfer should exist is exactly what Homung et al.²⁷ claim to have observed in their DC conductivity measurements of Si:P. Among other findings, these authors claim that below a majority dopant concentration of $2.78 \times 10^{18} \text{ cm}^{-3}$, (recall that $x_c = 3.52 \times 10^{18} \text{ cm}^{-3}$) the conductivity was better described by an activation process with an activation energy E_2 which was interpreted as a "hard" Hubbard gap.

Inspection of the $1.80 \times 10^{18} \text{ cm}^{-3}$ and $2.40 \times 10^{18} \text{ cm}^{-3}$ dopant concentration data presented in literature²⁷, which were analyzed as an activation process, show that the data spanned a very small temperature range. Our 69% sample corresponds to a dopant concentration very similar to the $2.40 \times 10^{18} \text{ cm}^{-3}$ dopant concentration sample in Ref. 29. Our DC conductivity results extended to 4.2 K. As indicated in Figure 3 a kink in the curve is clearly evident, which occurs at or somewhat below the lowest temperature indicated in the work from Homung et al.²⁷. The change in functional form that we observe is inconsistent with the presence of a hard gap which would result in a single activated process as the conduction mechanism. As we will show below, further evidence for the absence of a hard gap comes from the fact that we observe appreciable AC conductivity at frequency scales well below that of the purported gap energy.

B. AC Transport and Polarizability: The Crossover

Some of the most stunning and germane results from these investigations of electron-electron interactions in disordered systems are best summarized visually in Figure 9 in which the measured real part of the complex conductivity for the 69% and 50% samples are displayed as a function of frequency. The solid lines are linear and quadratic fits to the lower frequency and higher frequency data respectively, qualitatively displaying the expected behavior for a crossover from a Coulomb glass to a Fermi glass. The overlaid dotted lines are fits to the data using Eq. (12) and clearly this formula provides only a rough guide. The fit was made by forcing the linear portion to pass through the origin as well as the low frequency data and leaving the prefactor of the quadratic

portion as a free parameter. The crossover between linear and quadratic behavior is much more abrupt than the ES function predicts and is observed over our entire doping range. Such behavior was previously observed in an analogous disordered semiconductor system, SiB, for two very closely spaced doping levels near the MIT³.

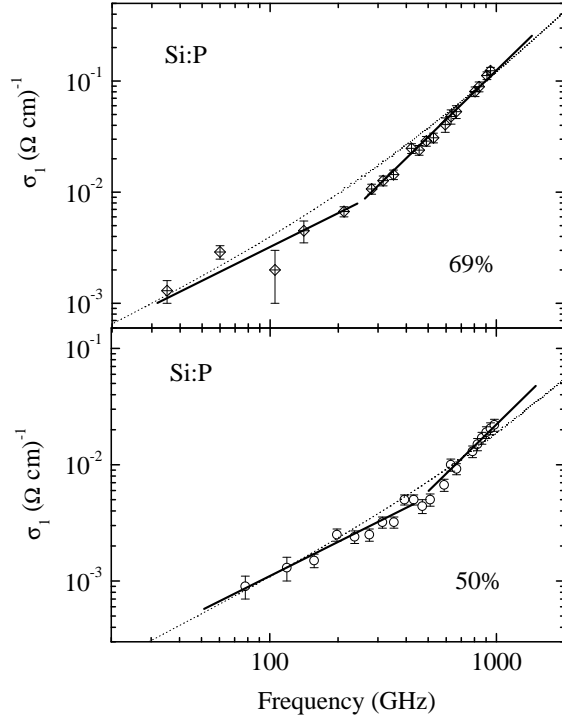


FIG. 9. The measured real part of the complex conductivity for the 69% and 50% Si:P samples as a function of frequency. The solid lines are linear and quadratic fits to the lower frequency and higher frequency data respectively qualitatively displaying the expected behavior for a crossover from a Coulomb glass to a Fermi glass. The overlaid dotted lines are fits to the data using Eq. (12).

The sharpness of the crossover is interesting in its own right and deserves further investigation as we do not here propose an explanation. This crossover in the real part of the complex conductivity was observed across our entire dopant concentration range except for samples very close to the MIT, where the crossover presumably occurs below our experimental frequency range. The experimentally determined crossover frequency, ω_c , plotted versus concentration in a functional form $1 - \frac{x}{x_c}$ is summarized in Figure 10.

The functional form in Figure 10, namely a power law in $1 - \frac{x}{x_c}$, is chosen because both the localization length, ξ , and the dielectric susceptibility of a sample near the MIT, namely $\chi = \chi_1 - \chi_2$, are either predicted to or have been experimentally shown to follow such a form. Fitting the crossover frequency to such a functional form we find

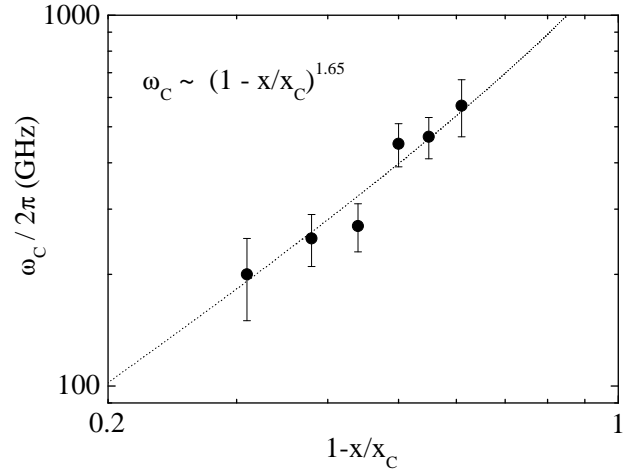


FIG. 10. The experimentally determined crossover frequencies for the various Si:P samples. The data is plotted against concentration in a functional form $1 - \frac{x}{x_c}$. We find $\alpha = 1.65$.

that ω_c is proportional to $1 - \frac{x}{x_c}$ where $\alpha = 1.65$. By comparing the concentration dependencies of the relevant energy scales to this experimentally determined power law we will show that the Coulomb interaction energy determines the crossover.

Recall that two energy scales have been set forth as being the energy scale at which the crossover from Fermi glass to Coulomb glass-like behavior is to occur. The original theoretical framework set forth by Efros and Shklovskii² has the Coulomb interaction energy U as the important energy scale. The second relevant energy scale in these systems is the Coulomb gap width, Δ . The evidence that the Coulomb gap is the pertinent energy scale of the system stems from an experiment performed by Lee et al.³. This report claims that it is not a gap in the single particle density of states, but rather a "dressed" Coulomb gap in the multiparticle density of states that determines the critical energy scale. Their claim, for which there does exist a theoretical framework²⁸, is that hopping phenomena occur due to multiparticle processes or polaronic effects, but that a Coulomb gap still forms in the density of states of these charge carrying entities. Nevertheless it is not unreasonable to believe that the dressed Coulomb gap should take a similar form to that of the ES single particle gap, Equation (7), as both are presumably caused by the same long range Coulomb interaction.

The dielectric constant enters into many of the germane formulae describing the electrodynamics of these disordered insulating systems. The effects of screening and polarization become more and more relevant as the MIT is approached. Therefore it is of fundamental importance to develop a theory that self-consistently takes into account the effects of the imaginary component of

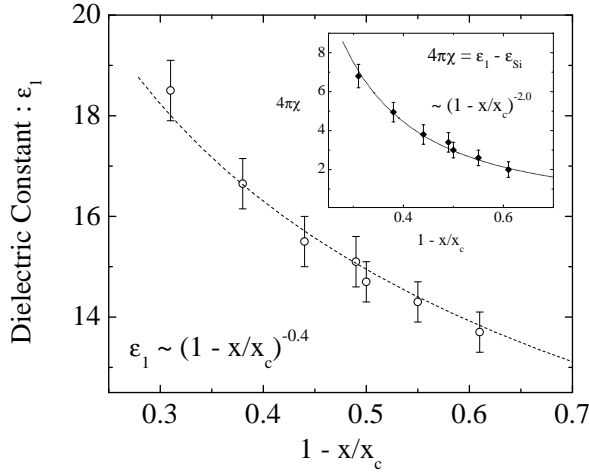


FIG. 11. The $T = 2.8$ K full measured dielectric constant ϵ_1 for the various SiP samples are plotted versus $1 - \frac{x}{x_c}$. The inset is that portion of the dielectric constant due to the disordered interacting system itself, $4\pi\chi$, obtained by subtracting off the background dielectric constant ϵ_{si} (of the host material silicon) from the full dielectric constant ϵ_1 . A clear divergence as a function of concentration is seen. These measurements are consistent with previous reports, and facilitate the analysis of the crossover energy scale.

the frequency dependent conductivity, i.e. the dielectric constant. As mentioned before, the immense advantage of our experimental techniques is the fact that we were able to separately measure both components of the complex conductivity. The full measured dielectric constant, as determined at $T = 2.8$ K, which is independent of frequency across our accessible frequency range (50 – 1000 GHz), is displayed in Figure 11. The inset shows that portion of the dielectric constant due to the disordered interacting system itself, which we refer to as the dielectric susceptibility of the disordered system, $4\pi\chi$, obtained by subtracting off the background dielectric constant ϵ_{si} (of the host material silicon) from the full dielectric constant ϵ_1 .

Measurements of the concentration dependent divergence of the dielectric constant are not new but having independently determined the values for our samples at these frequency ranges allows for more accurate analysis of the crossover energy scales. As a measure of confidence, when compared to previous experimental data on the dielectric susceptibility portion, namely $4\pi\chi$, of the full dielectric constant for SiP²⁹, which was found to take the form $\frac{x_c}{x} - 1$, with $\beta = 1.15$, we obtain from our data, when plotted and fitted in a similar fashion, a power also very close to unity, namely 0.96. However, measurements of the full dielectric constant, ϵ_1 , reported in the literature on SiB³⁰, a disordered insulator analogous to SiP, were fitted to a functional form of $1 - \frac{x}{x_c}$, and the power was found to be $\beta = 0.71$. We ob-

tain from our data, when plotted and fitted in a similar fashion, a power for $\epsilon_1 / 1 - \frac{x}{x_c}$ of $\beta = 0.38$, which is almost a factor of 2 different. This is perhaps accounted for by the fact that the materials have different dopant material. One must be cautious when analyzing the full dielectric constant in this latter manner as is found sometimes in the literature because there is a constant additive term due to the background dielectric constant of the host material Silicon $\epsilon_{si} = 11.7$ contained in the full dielectric constant $\epsilon_1 = \epsilon_{si} + 4\pi\chi$, and only at dopant concentrations very close to critical does one obtain $\epsilon_1 \approx 4\pi\chi$. Our subsequent analysis of the crossover energy between the non-interacting Fermi glass behavior and the electron-electron interaction dependent behavior of the Coulomb glass state is carried out using the latter normalized concentration functional form,

$1 - \frac{x}{x_c}$. It is therefore important to note here that as displayed in the inset of Figure 11, the dielectric susceptibility analyzed in this manner is found to obey the power law dependence, $4\pi\chi / 1 - \frac{x}{x_c}$, which presumably becomes the dominant power law dependence arbitrarily close to the MIT as the host material's ϵ_{si} becomes negligibly small. In fact such a trend can be seen in ϵ_1 in Figure 11, where at higher concentrations, namely the left-hand side of the figure, the slope tends to be steeper, as compared to the lower dopant concentrations on the right-hand side of the plot.

Utilizing the measured values of the full dielectric constant for each sample one can now analyze the crossover energy. We mention briefly that in our analysis we parameterize ϵ_c in terms of concentration. We acknowledge that the crossover energy should not scale as a power law over the whole doping range, but in our limited range modelling shows this to be an acceptable parameterization. Now let us first examine the Coulomb gap width.

The experimental data shows that the crossover frequency ω_c is proportional to $1 - \frac{x}{x_c}$ where from our analysis $\beta = 1.65$, and the full dielectric constant $\epsilon_1 / 1 - \frac{x}{x_c}$. Using these values and Eq. 7 one finds

that the DOS goes as $N_0 / 1 - \frac{x}{x_c}$. On the other hand the DOS can simply be estimated as $N_0 - x/W$, i.e. the dopant concentration divided by the bandwidth W , which could only show the correct behavior stated above if the bandwidth were increasing faster than the dopant concentration itself. It is quite unlikely that the DOS could have a concentration dependence that would make this explanation consistent with the measurements, but one cannot entirely rule out that the resulting concentration dependence is inconsistent with the Coulomb gap width as the DOS's concentration dependence is difficult to ascertain and the arguments provided above simply provide a reasonable estimate.

There is strong support however that the crossover en-

ergy is determined by the Coulomb interaction energy though. By setting the measured crossover energy scale equal to the Coulomb interaction energy we are able to determine both the magnitude of the localization length and the exponent with which it diverges as a function of concentration. Using an appropriate pre-factor for the overlap integral²⁰, $I_0 = 10^{13} \text{ s}^{-1}$, in the most probable hop distance term, $r_l = [\ln(2I_0/h!)]$, we find a localization length dependence as shown in Figure 12.

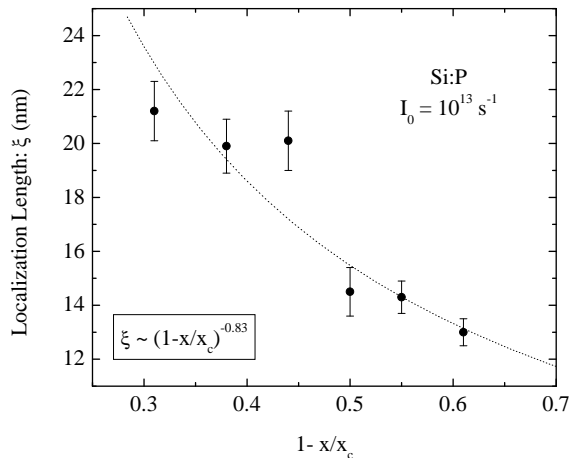


FIG. 12. Calculated localization length plotted versus $1 - \frac{x}{x_c}$ as determined from the measured crossover frequency energies. Our analysis entailed using an appropriate pre-factor for the overlap integral²⁰, $I_0 = 10^{13} \text{ s}^{-1}$ in the most probable hop distance term, $r_l = [\ln(2I_0/h!)]$.

The localization length exponent as shown in the figure is close to unity, the value originally predicted by Mott¹⁰, and the magnitude of the localization length is reasonable. The choice of the prefactor for the overlap integral may vary, but due to the fact that it is located within a natural logarithm term, even an order of magnitude variation greater or smaller than 10^{13} will result in a change of approximately a factor of two in the localization length. The consequent analysis for the localization length exponent, namely after changing I_0 by an order of magnitude both greater and smaller, still results in an exponent close to unity for both cases. It must be mentioned that some experimental results have indicated a localization length exponent closer to $\frac{1}{2}$, but these were found on the metallic side of the MIT using the zero temperature conductivity²⁹. These results strongly point towards the Coulomb interaction energy as being the energy scale at which the observed frequency dependent crossover from ES to Mott-like hopping conduction occurs.

Figure 13 offers a summary of various experimental data on different types of disordered insulating systems, including our own, of measured DC and AC crossover energies versus the normalized concentration parameter,

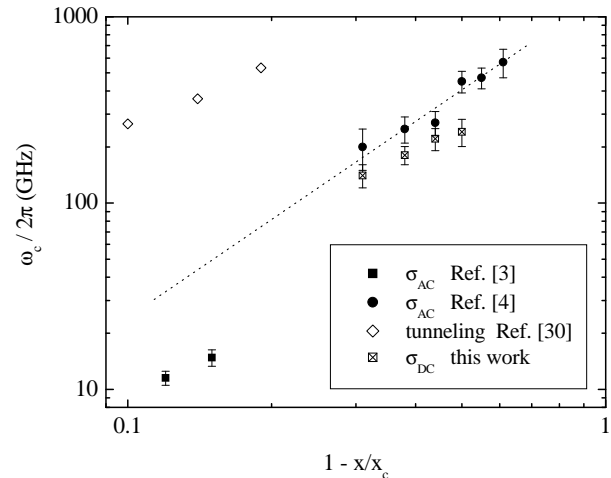


FIG. 13. Summary of various experimentally determined crossover energy scales determining the boundary between the interacting and non-interacting states of an electron glass system. The data represented by the open diamonds is adapted from tunnelling measurements³⁰ and the data represented by the full diamonds is adapted from AC conductivity network analyzer measurements performed in a dilution refrigerator³. Both measurements were done on SiB, a disordered insulator analogous to SiP. Our measured crossover frequencies⁴ are represented by the full circles and our experimentally determined crossover temperatures are converted to frequency and are represented by the crossed squares.

$1 - \frac{x}{x_c}$. The crossover energy for the various experimental techniques are converted to frequency and displayed in the figure as GHz. The data in the upper left of the figure displayed as open diamonds is the Coulomb gap width in the single particle DOS as determined by tunnelling measurements in SiB³⁰, a disordered insulator analogous to SiP. Although the Coulomb gap, speculated by Lee et al. to set the scale of the linear to quadratic crossover, was a smaller re-normalized or "dressed" one, on this plot the single particle gap sets an overall scale. One can see that the crossover energy is well inside the single particle Coulomb gap for all energies. The data in the lower left portion of the figure depicted by the full diamonds are crossover frequencies as determined by Lee et al. from AC conductivity measurements using a network analyzer and a dilution refrigerator in order to achieve quantum limit-like behavior on the same set of SiB samples as the above tunnelling data³. In their measurements, a sharp crossover analogous to our own observations was seen. The solid circles in Figure 13 represent the crossover frequencies as determined from our frequency dependent conductivity measurements on SiP. Our data extends the observed range of the sharp crossover deep into the insulating regime as the SiB measurements were closer to the critical concentration. The SiP and SiB data do not fall on the same line. This may be due to slight differences in these various disordered

system's dielectric constants or localization lengths. Finally the open crossed squares represent the crossover energies determined by us from our DC conductivity measurements. As can be seen the DC crossover data show a seemingly one-to-one correspondence to the observed crossover energies with the AC data. This in itself is a curious result, as the subsequent analysis of the DC data indicated that the observed crossover was not consistent with a crossover from Fermi glass Mott-like behavior to Coulomb glass ES-like behavior.

As a final note on the crossover data, recall that in the literature (see Ref. 29) one finds experimental DC conductivity data analyzed to indicate that in SiP below a certain dopant concentration, approximately $x=x_c = 80\%$, a "hard" Hubbard gap opens up. Having observed appreciable AC conductivity at frequencies below the purported hard gap energy, seems to rule out the possibility of a "hard" Hubbard gap, as the optical conductivity would be expected to drop precipitously to zero if such a gap were present. In fact it seems that the picture set forth by Efros and Shklovskii describing a crossover in the real part of the complex conductivity from a linear to quadratic dependence on frequency due to the effects of electron-electron interactions, seems to hold from very close to the quantum critical regime to deep within the disordered insulating electron glass system at least qualitatively if not quantitatively. From the expected form of $U(x)$, i.e. Eq. 11, and the reasonable behavior of the extracted σ_1 , it seems likely that the crossover is governed by the Coulomb interaction strength of a resonant pair as predicted by Efros and Shklovskii, but the sharper than expected behavior still needs to be explained.

C. AC Transport and Polarizability: The Coulomb Glass

Having established the fact that indeed a crossover in the real part of the frequency dependent complex conductivity occurs across a broad range of dopant concentrations in an archetypal model system of a disordered insulator, we wish to focus on the low energy limit of this electron glass system, i.e. the Coulomb glass. We will attempt to highlight successes and shortcomings of the theoretical predictions by drawing on the results of both the real and imaginary components of the complex conductivity of SiP and the previously reported results of another experimentally determined Coulomb glass, namely NbSi⁵. Comparing and contrasting the results of two Coulomb glasses, an amorphous highly doped metal-semiconductor alloy, NbSi, and a comparatively sparsely doped crystalline semiconductor, SiP, evidence for a general phase diagram of the Coulomb glass and the quantum critical region is revealed relative to our experimentally accessible window.

Figures 14 and 15 show the low energy magnitudes of the real and imaginary components of the complex frequency dependent conductivity plotted against frequency

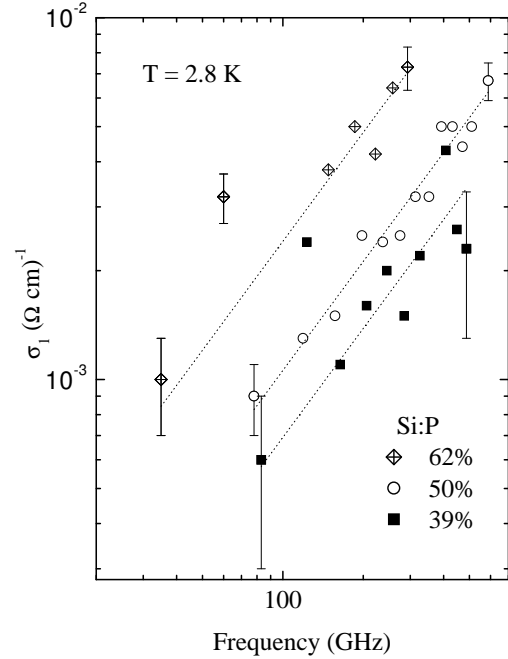


FIG. 14. The low energy, linear in frequency portion of the real part of the complex conductivity measured for three SiP samples plotted versus frequency. This data focuses on the Coulomb glass portion of electrodynamic response. The dashed lines are forced linear fits indicating self-consistency with the theory for a Coulomb glass, namely a linear frequency dependence and an increase in the magnitude of σ_1 with increasing dopant concentration.

for a number of SiP samples. These figures focus on the low frequency Coulomb glass data from the measurements of our experimentally accessible region of the optical conductivity. The dashed lines are linear fits to the data, highlighting two telltale characteristics of Coulomb glass-like behavior, namely a linear dependence of both components of the complex conductivity on frequency, and an increase in the magnitudes of both σ_1 and σ_2 with increasing dopant concentration. The error bars shown in Figure 14 are representative of all the data point's error bars; they show a general trend of increasing at lower frequencies both due to the logarithmic plot and the increasing difficulty in measuring such low conductivities. By contrast the error bars are much smaller and there is little scatter of the data points from the linear fits in Figure 15 because due to the inherent nature of an insulating system, the relative magnitude of the imaginary component is greater than the real component of the complex conductivity, and therefore falls in a range that can be measured more accurately and precisely.

Closer inspection of Figure 15 will reveal that the σ_2 data is linear across the entire measured spectral range, whereas the previous section clearly established a

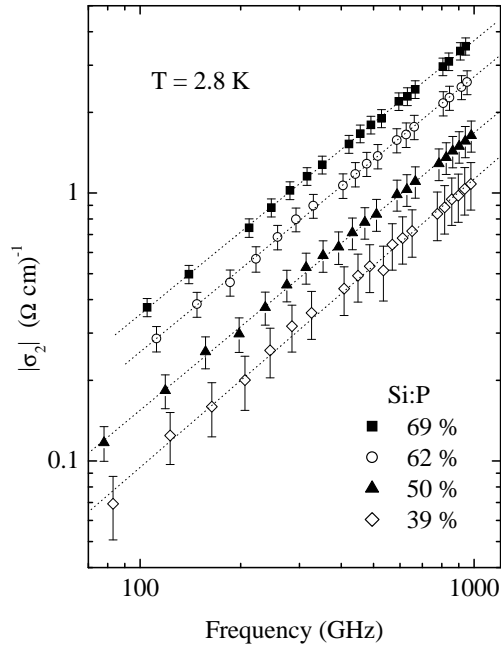


FIG. 15. The low energy, linear in frequency magnitude of the imaginary part of the complex conductivity measured for four Si:P samples plotted versus frequency. This data focuses on the Coulomb glass portion of electrodynamic response. The dashed lines are forced linear fits indicating self-consistency with the theory for a Coulomb glass, namely a linear frequency dependence and an increase in the magnitude of σ_2 with increasing dopant concentration.

crossover in σ_1 as a function of frequency. One might question whether this is physically acceptable on the grounds of Kramers-Kronig (KK) compatibility. This is established in Figure 16. This figure shows model data for σ_1 , plotted as the dotted line, on an arbitrary conductivity axis that via proper utilization of the Heaviside function mimics the Fermi glass to Coulomb glass-like crossover, namely a change in the frequency dependence of the real part of the complex conductivity from approximately linear to approximately quadratic, at the value of 10 on the arbitrary frequency scale. Above 100 on the arbitrary frequency scale a Lorentzian function is used to simulate a peak in the optical conductivity spectrum. The KK evaluated magnitude of σ_2 , resulting from the model data of σ_1 , is shown with the dashed curve. The imaginary component clearly displays a linear dependence on frequency, as evidenced by the shaded gray line, which is an aid to the eye for linear dependence, even though there exists an abrupt kink in the real part of the complex conductivity.

Having established that below the crossover frequency, both components of the complex conductivity follow an approximately linear frequency dependence allows us to

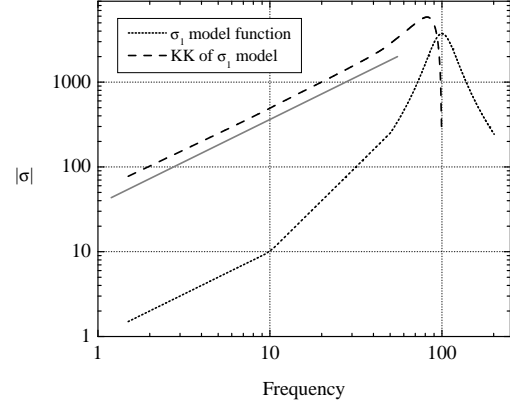


FIG. 16. A model function of $\sigma_1(\omega)$, the dotted curve, and the Kramers-Kronig calculated magnitude of $\sigma_2(\omega)$, the dashed curve, on axes of arbitrary conductivity and frequency. The model function for $\sigma_1(\omega)$ uses the Heaviside function to change from a linear dependence on frequency to a quadratic dependence at 10 on the arbitrary frequency scale. Above 100 on the arbitrary frequency scale a Lorentzian function is used to simulate a peak in the optical conductivity spectrum. The shaded gray line indicates a linear dependence.

analyze the full complex conductivity, $\hat{\sigma}$, using the following Kramers-Kronig compatible form,

$$\hat{\sigma} = \sigma_1 + i\sigma_2 = A(\omega) \quad (14)$$

$$= A(\omega) \cos \frac{\phi}{2} + iA(\omega) \sin \frac{\phi}{2} :$$

Such a dependence requires that the real and imaginary components follow the same power over a broad range of frequency and that this simple KK-compatible form only holds for $\phi = 1$, thus this is perfectly valid when analyzing the Coulomb glass regime. Given the functional form of the complex conductivity in Equation (14), one can very accurately determine the power of ϕ by taking the ratio of the magnitude of σ_2 and σ_1 to obtain what is commonly known as the phase angle of the complex conductivity

$$\phi = \frac{2}{\pi} \tan^{-1} \frac{j\sigma_2}{\sigma_1} : \quad (15)$$

The ratio of $j\sigma_2/\sigma_1$ and the subsequent power of ϕ was determined for each of the Si:P samples and the results are summarized in Figure 17. A similar analysis was performed on the insulating electron glass NbSiF₆, and the results from this Coulomb glass-like material are shown in the figure for comparison purposes. Panel (a) in Figure 17 shows the ratio of the magnitude of the imaginary to the real component of the complex conductivity for both Si:P and NbSiF₆.

It must be noted that the magnitude of the imaginary component plotted in the figure, for both Si:P and NbSiF₆, is that portion of the polarizability attributed to the interacting disordered electron system itself. Recall that

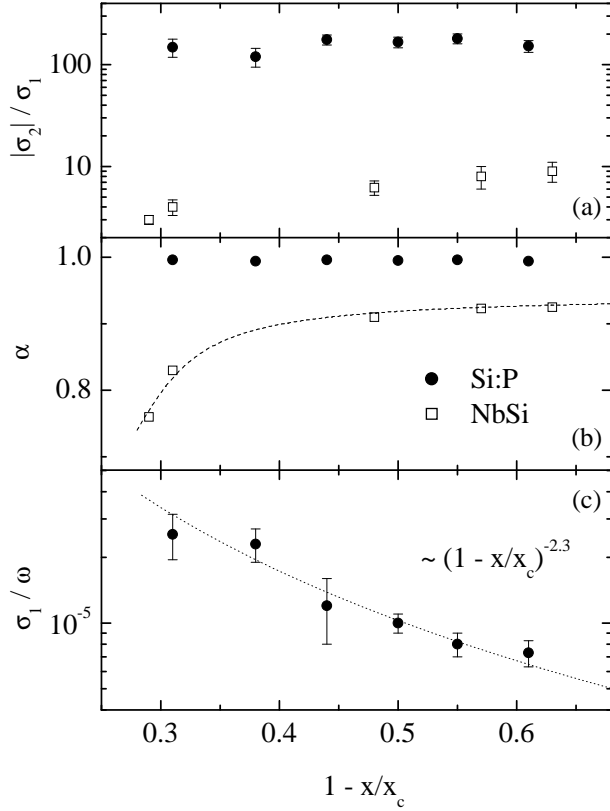


FIG. 17. Panel (a) shows the ratio of the magnitude of σ_2 to σ_1 for the two Coulomb glasses measured in this work, namely Si:P and amorphous NbSi. Panel (b) shows the calculated powers of σ as determined from Equation (15). The dashed line through the NbSi data is a guide to the eye showing an approach to the value $\frac{1}{2}$, as expected upon approaching the quantum critical regime. Panel (c) shows the divergence of the magnitude of σ_1 as a function of concentration.

the experimentally determined quantity is the full dielectric constant, $\epsilon_1 = \epsilon_{s1} + 4$. The imaginary component of the complex conductivity plotted in the figure has been calculated from the dielectric susceptibility portion χ'' , resulting from the electron-electron interactions via the relationship $j_2 j / (4 \epsilon_1)$. The ratio of $j_2 j / \epsilon_1$ using an imaginary component of the complex conductivity calculated from the full measured dielectric constant would necessarily diverge as the dopant concentration decreased, i.e. deep in the insulating regime, because $j_2 j$ would remain constant due to the static background dielectric constant from silicon itself, while ϵ_1 would continuously decrease.

Returning to panel (a) in the figure, we first note that this ratio for Si:P remains large and approximately constant across our range of dopant concentrations. From theory, one expects $j_1 j$ to be approximately equal to $j_2 j$ to within a factor of 2-5 (with a reasonable estimate for I_0) as predicted by Efros³¹. Applied to Si:P, Eq. (12)

in the $\hbar \omega < U(x_c)$ limit correctly predicts a linear correspondence between ϵ_1 and $j_2 j$, but the theory incorrectly predicts the measured proportionality by at least a factor of thirty. The proportionality is closer for NbSi but has a dependence on the doping concentration. This may be related to entering the quantum critical (QC) regime as discussed below. The magnitude of the ratio becomes even larger and the discrepancy greater if the full dielectric constant ϵ_1 is considered instead.

Panel (b) in Figure 17 shows the power as determined by Eq. (15) for both the amorphous NbSi and Si:P samples. The values for Si:P are approximately equal to, but slightly less than one, consistent with Figures 14 and 15. This indicates that the prefactor of the real and imaginary components of the complex conductivity for our samples of Si:P have the same concentration dependence across our entire range of dopant concentrations.

Panel (c) in Figure 17 shows the magnitude of the real part of the complex conductivity for the Si:P samples as the MIT is approached from the insulating side. This demonstrates that the prefactor A as set forth in Equation (14) can be written as a function of the normalized concentration, i.e. $A \propto (1 - \frac{x}{x_c})$ for Si:P. The prefactor of the imaginary component can be analyzed in a similar fashion and shows the same functional divergence as the real component, i.e. $(1 - \frac{x}{x_c})^{-2.3}$. This indicates that the real and imaginary components have the same concentration dependence consistent with the simple Kramers-Kronig form of the complex conductivity given in Equation (14). The fact that across a broad dopant range on the insulating side of the MIT we observe a similar divergence in both components of the complex conductivity for Si:P is in accordance with the concentration dependent theoretical predictions for photon assisted hopping conductivity², for excitations both within and larger than the Coulomb gap energy scale.

Still focussing on the Coulomb glass regime, the experimentally determined concentration dependence of the prefactor A , namely $(1 - \frac{x}{x_c})^{-2.3}$, as shown in panel (c) of Figure 17, can be used to determine which theoretically predicted functional form for the real part of the complex conductivity is more germane for our measured system. Recall that for photon energies smaller than the Coulomb gap width, i.e. excitations outside of the gap, the concentration dependent terms are summarized by the following: $\epsilon_1(\omega) = A / \frac{N_0^2 \omega^4}{\epsilon_1}$, and that for the alternate case, hopping conduction inside of the Coulomb gap one finds: $\epsilon_1(\omega) = A / \epsilon_1$. Having experimentally determined a parameterization for the concentration dependencies for both the full dielectric constant, $\epsilon_1 \propto (1 - \frac{x}{x_c})^{0.4}$, and the localization length, $\ell \propto (1 - \frac{x}{x_c})^{0.83}$, we find that the functional form for the prefactor is better described by photon-assisted hopping conduction occurring outside of the Coulomb gap. We find that $\epsilon_1 = \epsilon_{s1} / (1 - \frac{x}{x_c})^{2.9}$, which is not in exact agreement with our experimental findings for the prefactor (and in fact the density of states, N_0 term would make

this a slightly steeper function), but this is in much better agreement than the predicted concentration dependence of the prefactor for photon assisted hopping conduction inside the Coulomb gap.

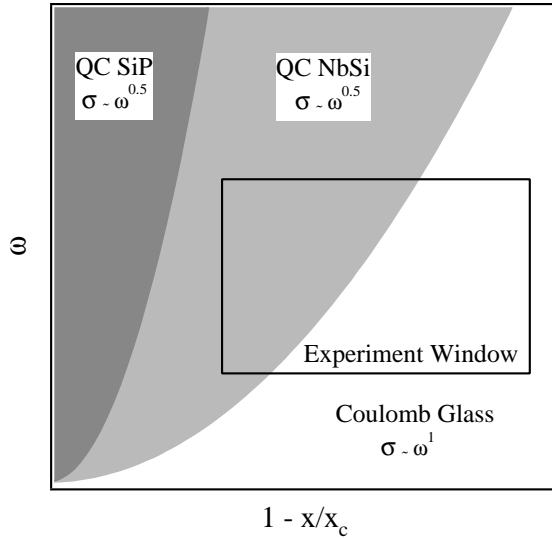


FIG. 18. A schematic of a possible phase diagram indicating the relative positions of the crossover energy scale to QC behavior vs. concentration of SiP and NbSi. The solid box indicates the "window" from which our experimental results are derived.

D. Quantum Critical Regime

When approaching the MIT from the insulating side, the frequency dependence is expected to cross over to the QC behavior^{6,32}, i.e. $\sigma_1 / \sigma_0 \propto \omega^{-1/2}$ in NbSi, when the localization length becomes comparable to the characteristic frequency dependent length scale, the dephasing length, ℓ_1 ¹², as discussed in Section II A. The crossover is not a phase transition and is not expected to be sharp. Therefore looking at a fixed window of frequencies, a broad, smooth crossover from $\sigma_1 / \sigma_0 \propto \omega^{-1/2}$ would show an averaged power of the frequency dependence similar to that measured for NbSi shown in the middle panel of Figure 17. The fact that we see an ω^{-1} across our whole doping range in SiP, but an $\omega^{-1/2}$ that approaches $\omega^{-1/2}$ in NbSi indicates that the critical regime in SiP is much narrower. Simple dimensional arguments³³ give a result similar to the non-interacting case⁹ that the crossover should be inversely proportional to the dopant DOS. The vastly smaller (a factor of 10^3) dopant density in SiP relative to NbSi is consistent with a narrower QC regime in SiP as compared to NbSi.

A schematic outlining our experimental window and the boundaries for the crossover from the insulating Coulomb glass regime to the QC regime in both SiP and NbSi versus a normalized concentration is shown in

Figure 18. The differently shaded regions indicate the relative positions of the crossover energy scale to QC behavior for SiP and NbSi. As mentioned above the crossover between the QC and the Coulomb glass regimes occurs when the localization length scale becomes comparable to the dephasing length scale, namely ℓ_1 , and from this relationship one finds that the crossover frequency is inversely proportional to the DOS⁹. This crossover then is expected to be narrower in SiP as compared to NbSi due to its smaller DOS. The crossover condition for the frequency in terms of the normalized concentration is

$$\omega_{QC} / \omega_0 \propto 1 - \frac{x}{x_c}^z \quad (16)$$

where the subscript QC refers to the quantum critical regime. The functional dependence is expected to be universal but the prefactor can vary from system to system. This then defines a condition for the crossover from QC to insulating glass-like behavior that depends only on the dynamical scaling exponent, z , and the localization length exponent, ν , that is consistent with experimental evidence. For the case of $z = 2$, and $\nu = 1$ as evidenced in NbSi⁶ and SiP⁴ respectively, the boundary would then have an approximately quadratic dependence on the normalized concentration as shown in Figure 18.

V. DISCUSSION

In analogy to the three phases of matter we are accustomed to dealing with in elementary physics, the solid, liquid and gas phases, a collection or assembly of electrons can be classified in a similar manner depending on the electrodynamic response of the system, each possessing an accompanying theoretical model. The room temperature response of a metal upon applying an electric field is well described by the Drude model. Here the electron system can be thought of as an electron gas with a temperature dependent mean free path and scattering time. An electron liquid would naturally be a system of electrons obeying Landau's theory of Fermi liquids^{34,35}. This successful theory has distinct hallmarks in the low energy limit. We shall investigate this low energy behavior more closely in the following section by comparing it to the low energy behavior of the materials we studied, generally classified as electron glasses.

The poorly understood and infrequently studied electron glasses might be considered a genre of the metal phase mentioned above, namely an electron solid, where the electronic states are localized due to disorder. The amorphous nature of the glassy state connotes disorder and hence this appellation was chosen to describe this type of assembly of electrons. Via our unique and versatile AC conductivity measurement techniques, and by investigating a series of disordered insulating systems proximal to a MIT, we have sufficient experimental evidence for electron glass systems to propose a classification scheme, i.e.

a ‘taxonomy’ for the electrodynamic response of electron glasses, along with a phase diagram containing appropriate crossover boundaries for the electron glass, Coulomb glass and quantum critical regimes.

A . On the Nature of the Coulomb Glass

One of the fundamental reasons for undertaking our investigations of these electron glasses is the surprising fact that even in a material as thoroughly studied as doped bulk silicon (due to the relevance of such research for the semiconductor industry), there exists no clear consensus as to the ground state and the nature of the low energy excitations in these disordered insulating systems. Using the frequency dependent complex conductivity we wished to probe the question as to whether or not the Coulomb interactions fundamentally change the ground state of the system. A philosophy that persevered for many years was that in analogy to the Fermi liquid theory, the theory describing the excitations at arbitrarily low energies in a system localized due to disorder, would indeed not be qualitatively influenced by electron-electron interactions³⁶. The theory created under this pretense was the one set forth by Mott¹, which gives an approximately quadratic frequency dependence of the real component of the complex conductivity. The coining of the appellation Fermi glass to describe this non-interacting disordered electron system was a direct consequence of the belief that there existed an analogy between the low energy electrodynamic of a Fermi liquid and this Fermi glass. Later, theoretical work and subsequent investigations of the DC conductivity lent credence to the import of long range interactions stemming from negligible screening of the low energy excitations, e.g. the work by Pollak^{14,28} and by Efros and Shklovskii².

In ‘many’ systems in solid state physics, this claim certainly is true, namely that the effects of correlations become simpler at low frequency or energy. The canonical example, as stated, is the Fermi liquid. The heavy-electron compounds such as CeAl₃ and UPt₃ are materials that have strongly correlated, yet delocalized charge carriers, and in the low energy limit, they follow the non-interacting Fermi liquid theory with renormalized parameters such as the effective mass and the relaxation rate³⁷. For these heavy-fermion systems there is a one to one correspondence between the low-lying excitations and those in a nearly free electron gas when the parameters of the latter, namely the mass and scattering rate, are properly renormalized to take into account the correlations. The name ‘heavy-electron’ stems from this effective enhanced mass (often several hundred times) which is a direct consequence of the electron-electron interactions, but nevertheless the theory describing the electrodynamic response of these systems is a non-interacting one.

On the other hand, our experimental data for both NbSi and SiP, two variants of electron glass systems,

show Coulomb glass-like behavior, i.e. a theory dependent on interactions, in the low energy frequency dependent electrodynamic response. Experiments done by another group on an electron glass system³, namely SiB, also show a linear in frequency power law dependence of the $T = 0; \omega \rightarrow 0$ conductivity supporting and verifying the import of electron-electron interactions in the low-energy response of these disordered systems. While this work on SiB reported on only two concentrations of dopant very close to the MIT, our further investigation across a broad range of dopant concentrations in SiP can confirm that this linear power law dependence continues deep into the insulating regime. Thus we have clear evidence that an interacting theory, namely that of a Coulomb glass, dependent on electron-electron correlations, is correct at the lowest experimentally accessible energy scales in these electron glass systems, in opposition to the original thoughts on the matter. Thus the Coulomb glass is a fundamental example in solid state physics as the non-interacting functional form is not recovered in the asymptotically low energy limit.

B . The Taxonomy of an Electron Glass

Now we focus on the electron glass phase as a whole with the intent of setting forth a universal framework for the AC response of such disordered insulating systems. In summary, we have observed Coulomb glass-like behavior across our entire range of doping concentrations in SiP and via a comparison with NbSi have arrived at a boundary condition consistent with our experimental data for the crossover from QC to Coulomb glass-like behavior, namely Equation (16). We have also established that a crossover from Fermi glass-like to Coulomb glass-like behavior exists, as is manifest in the experimental data of the real part of the complex frequency dependent conductivity, not only close to the MIT³, but also deep into the insulating electron glass regime. Employing these phenomenological results, namely that the power laws seen in the frequency dependent complex conductivity are qualitatively consistent with the three expected types of frequency dependent behavior theoretically postulated for the electron glass regime, we propose that the real component of the frequency dependent complex conductivity of these disordered insulators can be parameterized in general by

$$\sigma_1 / \omega \propto (\omega/x_c)^p \quad (17)$$

where the power p depends on the frequency and the dopant concentration. This classification scheme, or taxonomy, based on (ω/x_c) , captures the essential and germane physics of the electrodynamic response of electron glasses.

Figure 19 summarizes our proposed phase diagram and taxonomy on a plot of frequency versus the normalized concentration $(1 - \frac{x}{x_c})$. Recall that the criterion for

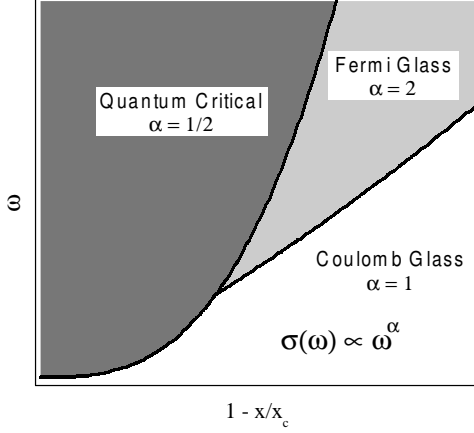


FIG. 19. This schematic of a possible phase diagram for an electron glass shows the regime boundaries for the QC, the Coulomb glass and the Fermi glass regimes in a two dimensional space of frequency versus normalized concentration $1 - \frac{x}{x_c}$.

the regime boundary condition for the crossover from Coulomb glass or Fermi glass-like behavior to the region where QC dynamics dominated was determined by Eq. (16). For a $z = 2$ theory and a localization length exponent $\nu = 1$, this crossover would go as $\omega_{qc} / (1 - \frac{x}{x_c})^2$ with a prefactor dependent on the dopant DOS. For the crossover from Fermi glass to Coulomb glass-like behavior, shown on the right hand side of the figure as the light gray and white regions respectively, we found that the crossover energy was more likely to be determined by the Coulomb interaction energy as opposed to the Coulomb gap width using concentration dependent arguments. Either way our experimentally determined crossover had the following concentration dependence, $\omega_c / (1 - \frac{x}{x_c})^{1.65}$. Here we must note that though the curve depicting this latter crossover, as shown in the figure, might intersect the QC crossover curve (depending on the material's energy scales), the QC regime will always take precedence. Recall that this crossover energy stems from a length scale argument that quantum critical behavior occurs when the electronic localization length, ξ , is greater than the dephasing length, ℓ . Ergo since both the Fermi glass and Coulomb glass behavior only occur in the opposite case, e.g. $\xi < \ell$, the length scale dependent crossover condition for QC behavior always dictates the low energy, close to critical behavior.

The classification of the power of ω / ω_c (Eq. 16), e.g. $\alpha = 1/2$ for QC dynamics, $\alpha = 1$ for Coulomb glass behavior and $\alpha = 2$ for Fermi glass behavior, provides more than just a taxonomy for these disordered insulating systems. For the latter two regimes, with powers 1 and 2 respectively, these numbers also represent the dimensions of phase space changing directly as \hbar^{-1} that these systems have access to for the creation of a real excitation.

In summary, we have presented results of our frequency dependent complex conductivity investigations into correlated electron phenomena in the electrodynamics of the electron glass SiP. The insulating side of the MIT displayed the expected power law dependencies for a Fermi glass and a Coulomb glass system with the latter being the low energy limit in our experimentally accessible window. In comparison with another electron glass, NbSi, with a distinctly different DOS, wherein we see a crossover from Coulomb glass-like behavior to quantum critical behavior, we have formulated a phase diagram based on phenomenological observations of all the predicted states for the insulating side of the MIT. The taxonomy for the electron glass that we have presented, is an attempt to both capture the essence of the physics and allow for a general description of the low energy frequency dependent electrodynamics of electron glasses.

A number of issues have also been left unresolved by this work. First of all, the apparent sharpness of the crossover in the real part of the frequency dependent conductivity cannot be explained by the current model of Efros and Shklovskii². Second, there certainly also exist further missing pieces with respect to the theories concerning the DC conductivity. For instance, the DC conductivity data does not seem to fit the Mott or ES predictions particularly well for our doping levels well into the insulating phase as indicated by the unphysical characteristic temperatures derived therefrom. Also, we have experimentally observed a crossover energy in the DC conductivity that is quite comparable to the crossover energy seen in the frequency dependent conductivity, and there is no reason within the canonical theory that there should be a correspondence in the AC and DC energy scales. Thirdly the experimentally determined ratio of the imaginary to the real component of the complex conductivity shows a deviation from the predicted ratio. Should a subsequent re-analysis of the theories pertaining to the electrodynamics of these electron glasses be undertaken, one should certainly include a self-consistent dynamic dielectric constant, and in a correct description, the proper ratios and relative sharpness of the crossovers must be manifest.

We are also hopeful that this work will plant the seed for further future investigations of other disordered insulating systems. For instance the samples used in these investigations were nominally uncompensated. Purposeful compensation will naturally redistribute many relevant energy scales. It would be of fundamental importance to investigate the veracity of the proposed taxonomy of the electron glass with respect to compensated systems. One must also note that our phase diagram stemmed from phenomenological observations of the three types of electron glass behavior, namely Fermi glass, Coulomb glass and quantum critical, but we would be remiss if we neglected to emphasize that we did not physically observe a

crossover from Fermi glass to quantum critical behavior, just the other crossovers that are possible in the taxonomy phase diagram. Needless to say, such an observation would be of great import in fully understanding electron glass behavior. Finally we have seen that in our experimental window, the original expectations set forth in the literature³⁶ have proven to be not realized, in that at our lowest accessible frequencies, an interacting theory is the germane one. This does not however rule out a subsequent change in the conduction mechanism at even lower frequencies, such as non-linear effects.

VII. ACKNOWLEDGEMENTS

We would also like to thank S. Kivelson, B. Shklovskii and E. Abraham s for useful discussions and also N. F. Mott who introduced one of us (GG) to the subject. This research was supported by the National Science Foundation grant DMR-0102405.

- ²⁵ G. G. Guner, *Millimeter and Submillimeter Wave Spectroscopy of Solids* (Springer Verlag, Berlin, 1998).
- ²⁶ P. Dai et al., *Phys. Rev. Lett.* **66**, 1914 (1991).
- ²⁷ M. Homung et al., *Physica Status Solidi (b)* **218**, 75 (2000).
- ²⁸ M. Pollak and M. Ortuno, in *Electron-Electron Interactions in Disordered Systems*, edited by A. L. Efros and M. Pollak (Elsevier, New York, 1985), pp. 287-408.
- ²⁹ H. F. Hess et al., *Phys. Rev. B* **25**, 5578 (1982).
- ³⁰ M. Lee et al., *Phys. Rev. B* **60**, 1582 (1999).
- ³¹ A. L. Efros, *Sov. Phys. JETP* **62**, 1057 (1985). An analogous three-dimensional form of the two-dimensional theory described in this paper can be derived.
- ³² H.-L. Lee et al., *Phys. Rev. Lett.* **80**, 4261 (1998).
- ³³ S. A. Kivelson, private communication.
- ³⁴ L. Landau, *Sov. Phys. JETP* **3**, 920 (1957).
- ³⁵ L. Landau, *Sov. Phys. JETP* **8**, 70 (1959).
- ³⁶ P. W. Anderson, *Comments S.S. Phys.* **2**, 193 (1970).
- ³⁷ A. M. Awasthi et al., *PRB* **48**, 10692 (1993).

-
- ¹ N. F. Mott and E. A. Davis, *Electronic Processes in Non-Crystalline Materials*, Second Edition, (Oxford University Press, Oxford, 1979).
 - ² A. L. Efros and B. I. Shklovskii, in *Electron-electron Interactions in Disordered Systems*, edited by A. L. Efros and M. Pollak (Elsevier New York, 1985), p. 409-482.
 - ³ M. Lee and M. L. Stutzmann, *Phys. Rev. Lett.* **30**, 056402 (2001).
 - ⁴ E. Helgren et al., *Phys. Rev. Lett.* **89**, 246601 (2002).
 - ⁵ E. Helgren et al., *Phys. Rev. Lett.* **87**, 116602 (2001).
 - ⁶ H.-L. Lee et al., *Science* **287**, 633 (2000).
 - ⁷ F. J. Wegner, *Zeitschrift für Physik B* **25**, 327 (1976).
 - ⁸ E. Abraham s et al., *Phys. Rev. Lett.* **42**, 673 (1979).
 - ⁹ B. Shapiro and E. Abraham s, *Phys. Rev. B* **24**, 4889 (1981).
 - ¹⁰ W. L. McMillan, *Phys. Rev. B* **24**, 2739 (1981).
 - ¹¹ D. Belitz and T. R. Kirkpatrick, *Rev. Mod. Phys.* **66**, 261 (1994).
 - ¹² S. L. Sondhi et al., *Rev. Mod. Phys.* **69**, 315 (1997).
 - ¹³ N. F. Mott, *J. of Non-Cryst. Sol.* **1**, 1 (1968).
 - ¹⁴ M. Pollak, *Disc. Far. Soc.* **50**, 13 (1970).
 - ¹⁵ V. Ambegaokar et al., *Phys. Rev. B* **4**, 2612 (1971).
 - ¹⁶ A. L. Efros and B. I. Shklovskii, *J. Phys. C* **8**, L49 (1975).
 - ¹⁷ V. L. Nguyen et al., *Sov. Phys., Semicond.* **13**, 1281 (1979).
 - ¹⁸ A. L. Efros et al., *S.S. Comm.* **32**, 851 (1979).
 - ¹⁹ S. Tanaka and H. Y. Fan, *Phys. Rev.* **132**, 1516 (1963).
 - ²⁰ Personal correspondence with B. I. Shklovskii. The I_0 used is determined by the Bohr energy of phosphorous.
 - ²¹ W. Teizer et al., *Phys. Rev. Lett.* **85**, 848 (2000).
 - ²² W. R. Thurber et al., *J. Electrochem. Soc.* **127**, 1807 (1980).
 - ²³ Y. Ootuka et al., *S.S. Comm.* **36**, 827 (1980).
 - ²⁴ A. Schwartz et al., *Rev. Sci. Instrum.* **66**, 2943 (1995).